Visualization of SHP-1–target interaction

Christoph Biskup[1,*], Annette Böhmer[2,*], Rico Pusch[2,*], Laimonas Kelbauskas[1], Alexander Gorshokov[3], Irina Majoul[3], Jörg Lindenau[4], Klaus Benndorf[1] and Frank-D. Böhmer[2,‡]

[1]Institute of Physiology II and [2]Research Unit Molecular Cell Biology, Medical Faculty, Friedrich Schiller University, Drackendorfer Str. 1, 07747 Jena, Germany
[3]Max-Planck Institute of Biophysical Chemistry, Am Fassberg 11, 37077 Göttingen, Germany
[4]Application Laboratory, Advanced Imaging Microscopy, Carl-Zeiss GmbH, Carl-Zeiss-Promenade 10, 07745 Jena, Germany
*These authors contributed equally to this work
‡Author for correspondence (e-mail: i5frbo@rz.uni-jena.de)

Summary

Signaling of receptor tyrosine kinases (RTKs) is regulated by protein-tyrosine phosphatases (PTPs). We previously discovered the efficient downregulation of Ros RTK signaling by the SH2 domain PTP SHP-1, which involves a direct interaction of both molecules. Here, we studied the mechanism of this interaction in detail. Phosphopeptides representing the SHP-1 candidate binding sites in the Ros cytoplasmic domain, pY2267 and pY2327, display high affinity binding to the SHP-1 N-terminal SH2 domain (K_d=217 nM and 171 nM, respectively). Y2327 is, however, a poor substrate of Ros kinase and, therefore, contributes little to SHP-1 binding in vitro. To explore the mechanism of association in intact cells, functional fluorescent fusion proteins of Ros and SHP-1 were generated. Complexes of both molecules could be detected by Förster resonance energy transfer (FRET) in intact HEK293 and COS7 cells. As expected, the association required the functional SHP-1 N-terminal SH2 domain. Unexpectedly, pY2267 and pY2327 both contributed to the association. Mutation of Y2327 reduced constitutive association in COS7 cells. Ligand-dependent association was abrogated upon mutation of Y2267 but remained intact when Y2327 was mutated. A phosphopeptide representing the binding site pY2267 was a poor substrate for SHP-1, whereas Ros activation loop phosphotyrosines were effectively dephosphorylated. We propose a model for SHP-1–Ros interaction in which ligand-stimulated phosphorylation of Ros Y2267 by Ros, phosphorylation of Y2327 by a heterologous kinase, and inactivation of Ros by SHP-1-mediated dephosphorylation play a role in the regulation of complex stability.

Key words: Protein-tyrosine phosphatase, SHP-1, Receptor tyrosine kinase, Ros, FRET

Introduction

Receptor tyrosine kinases (RTK) present an important class of signal transducers playing roles in development, regulation of cell proliferation, differentiation and apoptosis, as well as in diseases such as cancer and diabetes (Hunter, 1998; Schlessinger, 2000). Termination and fine-tuning of their signaling activity occurs through different mechanisms including phosphorylation by other protein kinases, internalization, degradation via the endosome or the ubiquitin-proteasome pathway and dephosphorylation by protein-tyrosine phosphatases (PTPs) (Chiarugi et al., 2002; Haglund et al., 2003; Östman and Böhmer, 2001; Schlessinger, 2000). Some of these processes, such as internalization and dephosphorylation, may also occur in concert (Haj et al., 2002). For many RTKs, these processes are not well understood. While it is clear that PTPs are biologically important negative regulators for at least some RTKs (Östman and Böhmer, 2001), little is known about the mechanisms and the specificity of these interactions. We have recently discovered an efficient interaction of the SH2 domain PTP SHP-1 with the RTK Ros (Keilhack et al., 2001). Ros is an epithelial RTK with a proven role in differentiation and regionalization of the epididymis; in addition, it has a transforming capacity (Riethmacher et al., 1994; Sonnenberg

et al., 1991; Sonnenberg-Riethmacher et al., 1996). Hyperphosphorylation of Ros in mice with impaired SHP-1 activity [motheaten viable (mev) mice] suggests that Ros signaling is attenuated by SHP-1 in vivo. SHP-1 binds directly to Ros and inhibits Ros signaling and Ros-dependent transformation in cell lines very efficiently (Keilhack et al., 2001). In order to elucidate the mechanism of Ros-SHP-1 interaction, we have characterized the binding of SHP-1 to Ros and the dephosphorylation of Ros by SHP-1 in more detail. Phosphopeptides representing the potential SHP-1 binding sites in the Ros C-terminal part pY2267 and pY2327 bind the SHP-1 N-terminal SH2 domain with high affinity. Both sites represent SHP-1 binding motifs, which are unique among RTKs. In intact cells, we observed FRET between a functional TrkA-Ros-ECFP fusion protein and EYFP-SHP-1 fusion proteins, provided that the N-terminal SH2 domain of SHP-1 was intact. Nerve growth factor (NGF), a functional ligand for the TrkA-Ros fusion proteins, stimulated the complex formation in intact cells as detectable by fluorescence lifetime imaging of TrkA-Ros-ECFP and membrane translocation of EYFP-SHP-1 fusion proteins. Ligand-dependent stimulation of complex formation required Ros pY2267, whereas Ros pY2327 mediated constitutive SHP-1 association. These results present the first example for visualizing interaction of SHP-1 with a target in intact cells.

Materials and Methods

DNA constructs

Blue fluorescent protein (BFPsg50) was fused to the C-terminus of the chimeric TrkA-Ros by amplifying the TrkA-Ros cDNA using HF-PCR (Roche) with suitable primers and inserting the product into pQB150-fN1 (Q-BIOgene) vector. In this construct, sgBFP and the Ros C-terminus are spaced by six glycine residues. To generate TrkA-Ros-ECFP, a DNA fragment coding ECFP with $MluI/EcoRI$ restriction sites in the ends was amplified by HF-PCR with pECFP-ER (Clontech) as template and exchanged for the BFPsg50 coding sequence in the TrkA-Ros-sgBFP construct. EYFP-SHP-1 fusion proteins were generated by cloning SHP-1 variants into pEYFP-C1 (Clontech) using HF-PCR and appropriate restriction to yield the constructs illustrated in Fig. 2A. In EGFR-Ros2267 the wild-type epidermal growth factor receptor (EGFR) sequence encompassing tyrosine 1173 (AEYLRV) was replaced by the Ros sequence encompassing tyrosine 2267 (LNYMVL) by generating a corresponding expression construct using PCR and standard cloning techniques (details available on request). All constructs were verified by DNA sequencing (MWG Biotech).

Peptides

All peptide syntheses were performed by Biosyntan (Berlin). Designation and sequence of the peptides is as follows: Ros2267 EGLNY$_{2267}$MVLATKSS-CONH$_2$, Ros2327 EGLNY$_{2327}$ACLAHSE-CONH$_2$, Epo429 DPPHLKY$_{429}$LYLVVSDSK-CONH$_2$. Cys2274 in the wild-type Ros sequence had to be replaced by a serine in the corresponding peptide Ros2267, because of the instability of the cysteine-containing peptide. In pRos2267, pRos2327 and pEpo429 the indicated tyrosine residues are phosphorylated. KKKK-Ros2267 and KKKK-Ros2327 contain four lysine residues at the N-terminus. To synthesize the biotinylated peptides Bio-pRos2267, Bio-Ros2267, Bio-pRos2327 and Bio-pEpo429 the peptides were coupled to Biotin using Fmoc-8-amino-3,6-dioxaoctanoic acid (Neosystem, France). pppRos (AREIpY$_{2103}$KNDpY$_{2107}$pY$_{2108}$RKRGEG-CONH$_2$) is a triple phosphorylated peptide corresponding to the Ros activation loop sequence amino acid 2099-2114.

Phosphatase assays

Activation assays for free SHP-1 were performed with pNPP as a substrate as described earlier (Keilhack et al., 1998). Dephosphorylation assays with synthetic phosphopeptides were done with a malachit green assay (Upstate Biotechnology) according to the manufacturer's instructions. Phosphopeptides were incubated at the concentrations indicated with 3 µg/ml recombinant SHP-1 catalytic domain glutathione-S-transferase (GST)-fusion protein at room temperature for 20 minutes.

Binding assays

GST-fusion proteins were purified as described earlier (Keilhack et al., 1998). For GST pulldown assays, HEK293 cells were transiently transfected with expression constructs for wild-type EGFR or EGFR Ros2267, and 200 µl lysate were used to perform GST pulldowns with 5 µg free GST (control) or 7 µg GST-SHP-1 N-SH2, as described earlier (Keilhack et al., 1998).

Surface plasmon resonance measurements were performed by Biaffin (Kassel, Germany) using a Biocore200 SPR-biosensor (BIAcore AB, Uppsala, Sweden). Biotinylated peptides were immobilized on a streptavidin-coated sensor chip (BIAcore AB) with a surface density of 40-170 resonance units (RU). All experiments were conducted at 22°C in running buffer (20 mM HEPES pH 7.4, 150 mM NaCl, 1 mM DTT, 0.005% Tween). GST-SHP-1 N-SH2 at concentrations ranging from 11 nM to 1.4 µM was injected over the sensor chip with a flow rate of 30 µl/minute for 5 minutes. Dissociation was measured during subsequent washing with running buffer for 5 minutes. The peptide surface was regenerated after every experiment by injection of 0.1% SDS in running buffer (20 seconds, 30 µl/minute). The signal obtained with the Ros2267-coated control surface shows no difference compared with an uncoated sensor chip and was subtracted from the signals obtained for the phosphopeptides. The data were analyzed using the BIAevaluation software 3.1 (BIAcore AB).

Cell culture, transfections and cell processing

Human embryonal kidney (HEK) 293 cells were grown in DMEM/F12 (Phenol-Red-free), COS7 cells in DMEM (Gibco), supplemented with 10% FCS (Gibco) in a humidified atmosphere at 37°C and 5% CO2. HEK293 cells were transiently transfected by using the calcium phosphate method as described earlier (Keilhack et al., 2001), COS7 cells with Lipofectamine Plus (Invitrogene), or Metafectene (Biontex) according to the manufacturer's instructions. Stable transfection of NIH3T3 cells with TrkA-Ros-sgBFP or TrkA-Ros-ECFP expression constructs was performed with Superfect or Effectene (Qiagene) according to the manufacturer's instructions and cells were selected in medium supplemented with 1 mg/ml G418 (Invitrogen).

If required, cells were starved in 0.5% FCS overnight, or 0% FCS for 6 hours and subsequently stimulated with 100 ng/ml NGFβ (Biomol) for the time indicated in the figure legends. Cells were extracted with lysis buffer containing 1% Triton X-100 or 1% NP40 plus protease and phosphatase inhibitors as described earlier (Keilhack et al., 2001).

Cell fixation for microscopy was performed with 4% paraformaldehyde in PBS and mounting with IMMUMOUNT solution (Shandon).

Functional assays and association experiments

Proliferation and focus formation assays were performed in a similar way to previous studies (Keilhack et al., 2001). To measure proliferation, 50,000 stably transfected or parental NIH3T3 cells/well were seeded into 6 well plates, cultivated in DMEM with 0.5% FCS with or without 50 ng/ml NGF. After 5 days, the cells were trypsinized and counted with a Casy 1 cell counter. For focus formation, cells were grown in the presence of 10% FCS for 14 days with a medium change every 2 days and were then stained with 0.5% crystal violet. To measure tyrosine phosphorylation and Erk-1/2 activation, cells were serum-starved for 6 hours and stimulated with 100 ng/ml NGF for 10 minutes. Aliquots of total cell lysates were subjected to immunoblotting with polyclonal anti-phosphotyrosine antibodies (BD Transduction Laboratories), or anti-pErk antibodies (Cell Signaling Technology). Expression levels were verified on stripped blots using anti-Ros (Riethmacher et al., 1994) and anti-panErk (Upstate Biotechnology) antibodies. Autophosphorylation of TrkA-Ros-sgBFP was measured after immunprecipitation as described by Riethmacher et al. (Riethmacher et al., 1994).

For testing association of TrkA-Ros fusion proteins with SHP-1 variants, coexpression was allowed for 24-48 hours and immunoprecipitation of TrkA-Ros was performed as described earlier (Keilhack et al., 2001) with anti-Ros antibodies or with monoclonal anti-GFP antibodies. Fluorescent fusion proteins were detected by immunoblotting using monoclonal anti-GFP antibodies (Santa Cruz Biotechnology) and untagged SHP-1 with polyclonal anti-SHP-1 antibodies (Santa Cruz). Tyrosine phosphorylation was detected with monoclonal anti-phosphotyrosine antibodies (4G10, Upstate Biotechnology).

To obtain active Ros kinase for phosphorylation of synthetic peptides, HEK293 cells, transiently transfected with TrkA-Ros in pcDNA3 were stimulated with 50 ng/ml NGF for 5 minutes at room temperature and lysed. Ros was immunoprecipitated and the immunoprecipitate was washed twice with 1% and once with 0.1%

Triton X-100 in kinase buffer (50 mM Hepes-HCl pH 7.4, 6 mM magnesium chloride, 100 µM sodium orthovanadate). For the kinase reaction 5 µl beads were added to 20 µl of reaction mixture containing the peptide KKKK-Ros2267 or KKKK-Ros2327 in concentrations ranging from 0.1-1 mM, 10 µM ATP and 0.25 µM [γ-^{32}P]ATP in kinase buffer. The reaction mixture was incubated at 30°C under shaking for 30 minutes and the reaction was stopped by addition of 5 µl 100 mM EDTA and 2.5 mg/ml BSA. The peptides were isolated from the reaction mixture and the incorporated radioactivity was measured as described earlier (Waltenberger et al., 1999). K_m was calculated using the software Enzyme kinetics 2.0.

Microscopy and spectroscopic measurements

To evaluate cellular distribution of ECFP and EYFP fusion proteins in living cells, confocal laser scanning microscopy (LSM) was performed with an inverted LSM 510 Rel. 1 (Carl Zeiss GmbH, Göttingen, Germany) using a Zeiss C-Apochromat 63× (NA 1.20) water immersion objective. ECFP and EYFP were excited with the 458 nm or 488 nm line of an argon ion laser, respectively. Fluorescence was recorded with a 475 nm long pass or a 505-550 nm band pass filter, respectively. EYFP-SHP1 translocations were recorded in living, transiently transfected COS7 cells with the same equipment. Expression of TrkRos-ECFP and various EYFP-SHP-1 variants was allowed for 24 hours, cells were serum-starved for 6 hours and then mock-treated or stimulated with 100 ng/ml NGF.

Fluorescence spectroscopy was carried out with transiently transfected, living COS7 cells as described previously (Majoul et al., 2001). About 1-3×10^6 cells were washed with PBS, gently removed from the surface into 1 ml of PBS and immediately used for recording spectra at 37°C using a Fluoromax-2 spectrofluorimeter. The donor (TrkA-Ros-ECFP) was excited at λ_{ex}=424 nm, and the acceptor (EYFP-SHPs) at λ_{ex}=494nm. The emission spectra of the donor (λ_{em}=450 nm-600 nm) and the acceptor (λ_{em}=510 nm-600 nm) were plotted and analysed using the Origin and Sigma Plot software.

Fluorescence lifetime measurements

Fluorescence lifetime measurements were performed as described previously (Biskup et al., 2004a; Biskup et al., 2004b). In brief, appropriate cells were selected with a confocal laser scanning microscope (Zeiss LSM 510 Rel. 2, Carl Zeiss GmbH, Göttingen, Germany) using a Zeiss C-Apochromat 63× (NA 1.20) water immersion objective. A mode-locked Titanium:Sapphire laser system (Mira 900, Coherent GmbH, Dieburg, Germany), which was pumped by a 5 W frequency doubled Nd:YVO$_4$ laser (5W Verdi, Coherent) and tuned to an emission wavelength of 860 nm, was used as excitation source. For streak-camera measurements, the pulse repetition rate was decreased to 2 MHz by a pulse picker (Model 9200, Coherent GmbH, Dieburg, Germany), whereas lifetime imaging was performed with the full repetition rate of 78 MHz. For both types of measurement, the second harmonic of the laser beam (430 nm) was generated in a β-barium borate (BBO) crystal and directed to the scan head of the LSM.

Fluorescence lifetime imaging

For the acquisition of fluorescence lifetime images the specimen was scanned continuously. Fluorescence light was directed to an external photomultiplier (MCP-PMT, 3809U-51, Hamamatsu), which was connected to a time-correlated single photon counting (TCSPC) module (SPC-730, Becker & Hickl, Berlin, Germany), where a 3D histogram of the photon density over spatial (x,y) and temporal (t) coordinates was built up.

Streak camera measurements

The LSM scanning software was used to direct the laser beam to a spot of interest. Fluorescence was guided via an optical fiber to a spectrograph (Model 250is, Chromex, Albuquerque, NM) and a streak camera (Model C5680 with S20 photocathode and M5677 sweep unit, Hamamatsu Photonics Deutschland, Herrsching, Germany).

Data analysis

Streak images were analyzed with our own software, whereas TCSPC data were analyzed with a commercial software package (SPCImage V2.4, Becker & Hickl). Both software versions used the 'iterative reconvolution method' in order to recover the lifetime from the fluorescence decay. A modified Gauss-Newton algorithm was used to approximate the data obtained for one pixel by a mono- or biexponential decay function. The goodness of a fit was judged by the value of the reduced χ_v^2. A model was rejected when χ_v^2 exceeded 1.5. In case of a biexponential fit, amplitude-weighted mean lifetimes (τ_m) were calculated according to $\tau_m = A_f\tau_f + A_s\tau_s$, where A_f and A_s are the relative amplitudes of the fast and slow lifetime component, respectively. Mean lifetimes (τ_m^c) for a cell were calculated by averaging over the amplitude-weighted mean lifetimes ($\tau_{m,i}$) of all pixles (i) taking into account their intensity (I_i):

$$\tau_m^c = \sum_i I_i \tau_{m,i} \Big/ \sum_i I_i \ .$$

Mean lifetimes

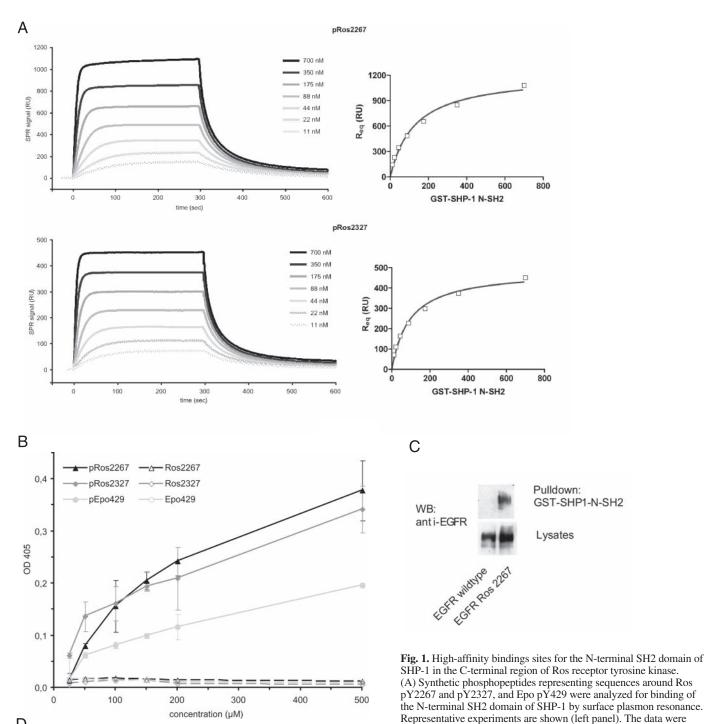$$\left(\overline{\tau_m^c} = \sum_j^n \tau_{m,j}^c \Big/ n \right)$$

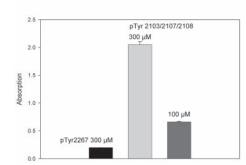for a series of measurements (j) are presented as mean±s.e.m.

Results

The N-terminal SHP-1 SH2 domain binds with high affinity to Ros phosphotyrosines 2267 and 2327

According to previously obtained biochemical data, the interaction between Ros and SHP-1 in vitro required the SHP-1 N-terminal SH2 (SHP-1-N-SH2) domain and Ros pY2267. The features of this interaction suggested that it occurs with high affinity (Keilhack et al., 2001). We therefore determined binding constants for Ros-derived phoshopeptides and the SHP-1 N-terminal SH2 domain using surface plasmon resonance measurements (Fig. 1A). An earlier characterized efficient binding sequence on the human erythropoietin receptor (EpoR), pY429 (Klingmüller et al., 1995), was used for comparison. SHP1-N-SH2 binds to the EpoR-derived phoshopeptide with a K_d of 1960 nM (Table 1), which is close to previously reported values (Beebe et al., 2000; Pei et al., 1996). The phosphopeptide representing the Ros pY2267 site bound SHP1-N-SH2 with a K_d of 217 nM, i.e. with an affinity almost one order of magnitude higher. Thus, Ros pY2267 represents one of the best binding sites for SHP-1 characterized to date. Two further candidate binding sites for SHP-1 exist in the C-terminus of Ros, pY2166 and pY2327. Previous mutational analysis showed that both are apparently not significantly contributing to the SHP-1 Ros association in vitro (Keilhack et al., 2001). Peptides representing these sites were also subjected to binding assays. While Ros pY2166 exhibited little binding (not shown), Ros pY2327 bound with a K_d of 171 nM, i.e. with an affinity similar to Ros pY2267. The efficient interaction of Ros pY2267 and 2327 with SHP1-N-SH2 is further supported by SHP-1 activation assays (Fig. 1B). Phosphopeptide ligands of SHP1-N-SH2 are known to activate

A

B

C

Fig. 1. High-affinity bindings sites for the N-terminal SH2 domain of SHP-1 in the C-terminal region of Ros receptor tyrosine kinase. (A) Synthetic phosphopeptides representing sequences around Ros pY2267 and pY2327, and Epo pY429 were analyzed for binding of the N-terminal SH2 domain of SHP-1 by surface plasmon resonance. Representative experiments are shown (left panel). The data were fitted to determine the kinetic constants k_{ass} and k_{diss} depicted in Table 1. Signals at equilibrium were also determined and plotted against concentrations (right panel). Dissociation constants determined by this procedure are also given in Table 1. (B) The same set of peptides was used for activation experiments. Recombinant SHP-1 was incubated with different concentrations of the phosphopeptides and activity was then determined with pNPP as a substrate. (C) Wild-type EGFR and an EGFR with the sequence around Ros pY2267 ($LNY_{2267}MVL$) inserted in place of the EGFR pY1173 ($AEY_{1173}LR$) were overexpressed in HEK293 cells and cell lysates were subjected to a pulldown with a GST-fusion protein of the SHP-1 N-terminal SH2 domain. Affinity-precipitated receptor is visualized by immunoblotting with anti-EGFR antibodies. (D) Phosphopeptides representing the sequence around pY2267 or activation loop phosphotyrosines pY2103, pY2107 and pY2108 were subjected to a phosphatase reaction with the catalytic domain of SHP-1. Phosphate release was determined with Malachite Green. Note that the more efficient dephosphorylation of the activation loop phosphopeptide is also obvious at matched concentrations of phosphotyrosine (100 µM activation loop phosphopeptide versus 300 µM pY2267 peptide).

D

Table 1. Binding constants for the N-terminal SH2 domain of SHP-1

Peptide	k_{ass} $(10^5\,M^{-1}\,s^{-1})$	k_{diss} $(10^{-2}\,s^{-1})$	K_d (k_{diss}/k_{ass}) (nM)	K_d (steady state) (nM)
pRos2267	1.6	3.4	217	128±22
pRos2327	2.1	3.6	171	94±14
pEpo429	ND	ND	ND	1960±270

The data were obtained by surface plasmon resonance measurements. ND, not determined. Kinetic data were in agreement with those obtained by calculation from steady state but, due to considerable noise, fitting was not sufficiently reliable.

SHP-1 since the binding releases SHP-1 from an inhibited conformation (Pei et al., 1994; Pei et al., 1996; Yang et al., 2002). Again, peptides representing Ros pY2267 and pY2327 activated SHP-1 much more effectively than the EpoR-derived phosphopeptide (Fig. 1B). We finally proved high affinity-binding of SHP-1 to Ros pY2267 by transferring the site to another RTK. We have previously shown that SHP-1 can bind to the epidermal growth factor receptor (EGFR) and that both SH2 domains are required for binding (Keilhack et al., 1998). SHP1-N-SH2 alone cannot bind to EGFR (Keilhack et al., 1998). When the sequence around pY1173 in the EGFR C-terminus was engineered to the sequence around Ros pY2267, the modified EGFR now acquired the ability to bind SHP1-N-SH2 (Fig. 1C). Thus, Ros pY2267 is sufficient to confer high affinity interaction with SHP1-N-SH2 also in the context of another RTK.
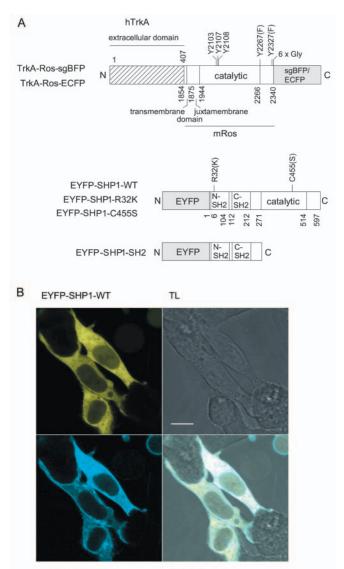
The question arose why mutation of Ros Y2327 has little effect on SHP-1 binding in vitro, despite the high affinity of the corresponding phosphopeptide to the SHP-1 SH2 domain. One obvious possibility would be the poor phosphorylation of this site. We, therefore, tested the capacity of Ros kinase to phosphorylate peptides corresponding to Ros Y2267 and 2327. Interestingly, the Ros Y2267 peptide was efficiently phosphorylated (K_m 0.14 mM) while the Ros Y2327 peptide was not ($K_m \gg 1$ mM, not shown). Thus, in vitro Ros Y2327 may not function as a high-affinity SHP-1 binding site because of an inefficient phosphorylation by Ros kinase.

It has previously been proposed that SHP-1 is highly active against its own SH2 domain binding site(s) (Bone et al., 1997) leading to decomposition of SHP-1-substrate complexes. We tested this hypothesis for Ros and SHP-1 by measuring activity of the isolated catalytic domain of SHP-1 against
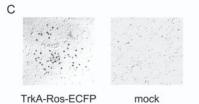
phosphopeptides corresponding to different Ros phosphorylation sites. These assays revealed that SHP-1 can dephosphorylate the binding site pY2267 phosphopeptide but with only low efficiency (Fig. 1D). By contrast, efficient dephosphorylation was detectable for the activation loop phosphopeptide containing pY2103, 2107 and 2108 (Fig. 1D). These data suggest that SHP-1 may destabilize the complex with Ros not primarily by dephosphorylation of binding site(s), but rather by inactivation of the Ros kinase.

Fluorescent Ros and SHP-1 derivatives are functional

The high affinity of interaction between Ros and SHP-1

Fig. 2. Structure and expression of TrkA-Ros and SHP-1 fluorescent fusion proteins. (A) Schematic presentation of fluorescent fusion protein constructs. Ros is used as a TrkA-Ros chimerical protein, which allows stimulation of the kinase by nerve growth factor (NGF). Protein domains and important amino acid residues are indicated. (B) Expression of TrkA-Ros-ECFP and EYFP-SHP1-WT in HEK293 cells. TL, transmitted light; bar, 10 μm. (C) Localization of TrkA-Ros-ECFP in the plasma membrane of HEK293 cells shown by immuno-electron microscopy. Membranes of HEK293 cells expressing TrkA-Ros-ECFP and wild-type SHP-1, or mock-transfected cells for control, were freeze-fractured and TrkA-Ros-ECFP was detected with anti-GFP antibodies, followed by immuno-gold labeled secondary antibody. The inner plasma membrane surface, identified by morphological criteria, is shown. Outer surfaces, nuclear membrane or mitochondria showed no labeling (not depicted).

encouraged us to attempt to visualize this interaction in intact cells. To this end, fusion proteins of different SHP-1 variants with enhanced yellow fluorescent protein (EYFP) were constructed (Fig. 2A). Since the ligand of Ros is still unknown, a chimeric protein was employed, consisting of the TrkA NGF-receptor extracellular domain and Ros transmembrane and intracellular domain (Riethmacher et al., 1994). This protein was fused at the C-terminus either to a modified blue fluorescent protein (sgBFP) or to an enhanced cyan fluorescent protein (ECFP) (Fig. 2A). Expression of these fusion proteins in HEK293 cells showed localization in both intracellular membranes and in the plasma membrane (Fig. 2B). Localization of a fraction of TrkA-Ros fusion protein in the plasma membrane was further supported by immuno-electron microscopy (Fig. 2C). As described earlier (Tenev et al., 2000), fluorescent SHP-1 fusion proteins localize largely in the cytoplasm (Fig. 2B). Functionality of TrkA-Ros and SHP-1 fusion proteins was first tested in transient expression experiments. All fusion proteins were expressed with the expected size. Tagged TrkA-Ros expression in HEK293 cells led to abundant tyrosine phosphorylation of multiple proteins, comparable with expression of wild-type TrkA-Ros. Expression of full-length intact EGFP-SHP1 together with TrkA-Ros suppressed tyrosine phosphorylation, demonstrating that the PTP is active (data not shown). To further prove the functionality of the tagged TrkA-Ros, we established stable NIH3T3 cell lines expressing TrkA-Ros-sgBFP or TrkA-Ros-ECFP. As shown in Fig. 3, ligand-dependent activation of (1) TrkA-Ros autophosphorylation, (2) Erk1/2, (3) cell proliferation, and (4) focus formation could be demonstrated in cells stably expressing tagged TrkA-Ros, similar to that described earlier for NIH3T3 cells expressing TrkA-Ros (Riethmacher et al., 1994). In several assays, some constitutive TrkA-Ros activity was detectable in the absence of NGF, which may be related to overexpression of TrkA-Ros.

Formation of Trk-Ros-SHP-1 complexes in intact cells

To assess complex formation between Ros and SHP-1 in intact cells, we checked whether FRET could be observed between TrkA-Ros-ECFP and different coexpressed EYFP-SHP-1 variants.

FRET occurs when a donor molecule is brought into close vicinity (<10 nm) of a suitable acceptor molecule. In this case, the excited donor molecule can transfer its excitation energy to the acceptor molecule. In turn, the intensity and the lifetime of the donor fluorescence decreases, and the acceptor fluorescence increases. We measured changes in the fluorescence lifetime of the donor molecule because this approach has, in contrast to fluorescence intensity measurements, the advantage of being independent of donor and acceptor concentrations.

One of the techniques used in this study to measure fluorescence lifetimes consists of a combination of a spectrograph and a streak camera. This setup allows so-called streak images to be recorded, from which both fluorescence spectra and fluorescence decay curves can be extracted (Biskup et al., 2004b). Fig. 4A shows typical fluorescence emission spectra (upper panel) and fluorescence decay curves (lower panel) obtained from HEK293 cells expressing TrkA-Ros-ECFP only (blue curve) and from

HEK293 cells coexpressing TrkA-Ros-ECFP and SHP-1 variants. Compared with the spectrum of TrkA-Ros-ECFP alone, the spectrum obtained from cells coexpressing TrkA-Ros-ECFP and EYFP-SHP1-SH2 (green curve) shows that the donor (CFP) fluorescence in the wavelength range between 465 and 495 nm was decreased, whereas the acceptor (YFP) fluorescence between 520 and 540 nm was increased. Furthermore, the fluorescence decay of the CFP moiety was accelerated upon coexpression with EYFP-SHP1-SH2. Whereas the
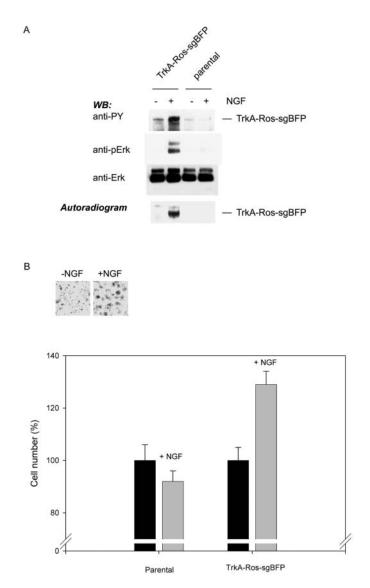

Fig. 3. Fluorescent TrkA-Ros fusion proteins are functional. (A) A fluorescent TrkA-Ros fusion protein signals in response to NGF. Stable NIH3T3 cell lines expressing TrkA-Ros-sgBFP were subjected to NGF stimulation as indicated and TrkA-Ros-sgBFP autophosphorylation and Erk1/2 activation were detected by immunoblotting with lysate aliquots (upper panels). TrkA-Ros-sgBFP autophosphorylation was also measured with immunopreciptated receptor (lower panel). Experiments with the parental cells are shown for comparison. (B) A fluorescent TrkA-Ros fusion protein transduces biological signals. NIH3T3 cells, stably expressing TrkA-Ros-sgBFP, were stimulated with NGF as indicated, and focus formation (upper panel) or proliferation (lower panel) were assessed.

fluorescence decay of ECFP or TrkA-Ros-ECFP could be fitted by a monoexponential function yielding a lifetime of 2.03±0.11 ns (nanoseconds), the ECFP fluorescence decay recorded from cells coexpressing TrkA-Ros-ECFP and EYFP-SHP1-SH2 had to be approximated by a biexponential function, yielding a mean fluorescence lifetime of 1.15±0.06 ns. A similar lifetime was observed for the EYFP-SHP1-C455S mutant (Table 2). Importantly, ECFP lifetimes for TrkA-Ros-ECFP were significantly longer when it was coexpressed with EYFP-SHP-1 variants with a defective N-terminal SH2 domain (EYFP-SHP1-R32K) (Fig. 4A, lower panel, Table 2). These results indicate a pronounced constitutive association of TrkA-Ros-ECFP with SHP-1 fusion proteins in overexpressing
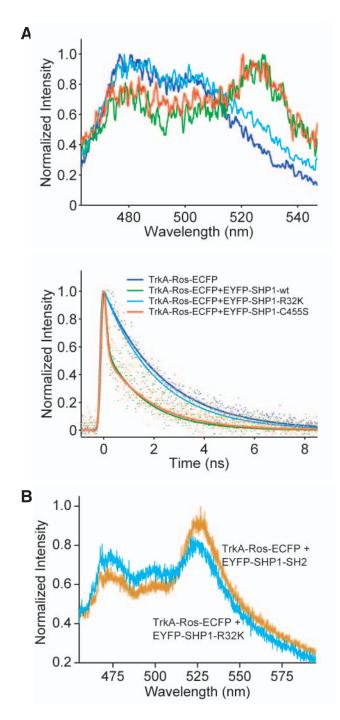
Table 2. Fluorescence lifetime of TrkA-Ros-ECFP in the presence of different EYFP-SHP-1 fusion proteins

Interaction partner of TrkA-Ros-ECFP	Fluorescence lifetime (ns)
EYFP-SHP1-WT	1.15±0.06
EYFP-SHP1-C455S	1.29±0.08
EYFP-SHP1-SH2	1.31±0.07
EYFP-SHP1-R32K	2.00±0.05

Lifetimes were measured in HEK293 cells transiently coexpressing TrkA-Ros-ECFP and one of the indicated fusion proteins. The lifetime for free ECFP was determined as 2.03±0.11 ns. Values were compiled from intracellular regions in different cells and means±s.e.m. are given. In the presence of all SHP-1 fusion proteins with intact N-SH2 domain, the lifetimes were significantly different from the lifetime in the presence of EYFP-SHP1-R32K (Student's t-test, $P<0.002$).

HEK293 cells which requires an intact N-terminal SH2 domain.

Consistent with these results obtained in individual HEK293 cells, a constitutive association was also indicated by spectra obtained from transfected living COS7 cells. For these experiments, cells were removed from the cell culture dish, suspended in PBS and subjected to fluorescence spectroscopy (Majoul et al., 2001) (Fig. 4B). Again, cells coexpressing TrkA-Ros-ECFP and EYFP-SHP1-SH2 showed a decrease of donor (ECFP) fluorescence and a corresponding increase in acceptor fluorescence (EYFP) compared with cells expressing identical amounts of EYFP-SHP1-R32K (estimated by excitation of EYFP).

Visualization of ligand-stimulated complex formation

To visualize ligand-stimulated complex formation, a different method based on time-correlated single photon counting (TCSPC) was used to measure fluorescence lifetimes in COS7 cells transfected with different variants of TrkA-Ros-ECFP and EYFP-SHP1-SH2 (Biskup et al., 2004a). The technique is based on a 3D histogramming process that records photon density over both time and spatial coordinates of the scanning area. Fluorescence decays recorded in each pixel were approximated by a mono- or a biexponential function and mean

Fig. 4. Constitutive association of TrkA-Ros and SHP-1 in intact cells. (A) Association of TrkA-Ros and SHP-1 in HEK293 cells demonstrated by streak camera measurements. TrkA-Ros-ECFP was coexpressed with different EYFP-SHP1 variants as indicated. Fixed cells were excited at 430 nm and emitted fluorescence was recorded by a combination of a spectrograph and a streak camera. Typical examples of fluorescence emission spectra (upper panel) and fluorescence decay curves in the wavelength range from 465-495 nm (lower panel) that were calculated from the recorded data (streak images) are shown. Cumulated data are presented in Table 2. (B) Detection of constitutive interaction between TrkA-Ros-ECFP and EYFP-SHP-1 by fluorescence spectroscopy. TrkA-Ros-ECFP was coexpressed with the EYFP-SHP1-SH2 or EYFP-SHP1-R32K fusion proteins, as indicated, in COS7 cells. Cells were suspended and spectra were recorded in a fluorescence spectrophotometer with excitation at optimal wavelength for ECFP (λ_{ex}=424 nm). EYFP spectra (λ_{ex}=494 nm) were recorded in the same samples and revealed that the amount of EYFP constructs in both sets of cells was identical (not shown).
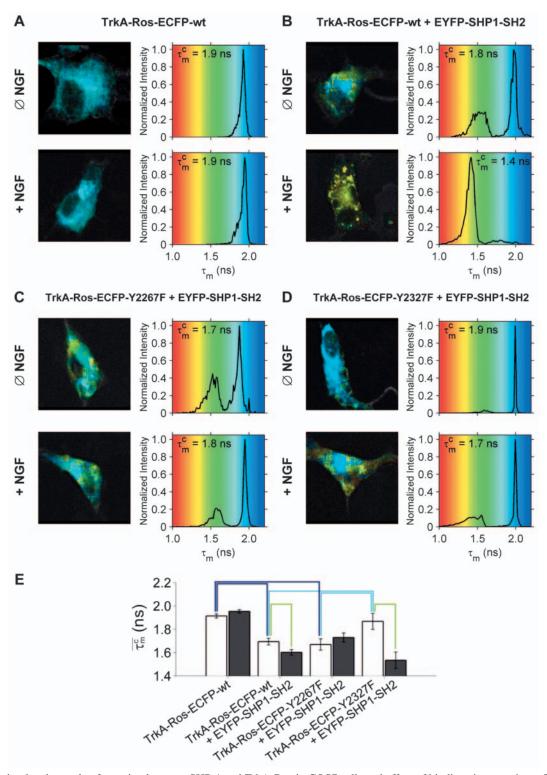
Fig. 5. Ligand-stimulated complex formation between SHP-1 and TrkA-Ros in COS7 cells and effect of binding site mutations. COS7 cells expressing TrkA-Ros-ECFP, or TrkA-Ros-ECFP mutants together with EYFP-SHP1-SH2 as indicated, were starved in serum-free medium for 6 hours and were either left untreated or were stimulated with 100 ng/ml NGF for 20 minutes. Thereafter, the cells were fixed and subjected to fluorescence lifetime imaging. (A-D) Left panels: fluorescence lifetime images. Amplitude weighted mean lifetimes (τ_m) were color coded as indicated in the right panels. Right panels: distribution of mean lifetimes over the entire cell. The mean fluorescence lifetime τ_m^c was calculated by averaging over all pixels of the cell taking into account their relative intensity. (E) Bar graph of the mean of the fluorescence lifetimes ($\overline{\tau_m^c}$) determined in 5-11 cells. White bars represent measurements in the absence, and grey bars in the presence of NGF. Error bars represent the standard error of the mean. Significant (Student's *t*-test, $P<0.05$) differences between the data sets are marked by brackets. Green brackets mark a significant decrease of mean lifetimes that can be attributed to NGF. Dark and light blue brackets indicate data sets that reflect significant changes in constitutive association.

lifetimes (τ_m) were encoded by color as indicated in the figure legends.

The fluorescence decays recorded from COS7 cells expressing ECFP or TrkA-Ros-ECFP alone could be approximated in all pixels by a monoexponential decay function, yielding a mean of fluorescence lifetimes for all cells ($\overline{\tau_m^c}$) of 2.02±0.03 ns and 1.91±0.02 ns, respectively. Moreover, fluorescence lifetimes do not differ throughout the cell as shown by the fluorescence lifetime image of a cell expressing TrkA-Ros-ECFP alone (Fig. 5A). Thus, the lifetime of ECFP does not change when it is fused to proteins, nor does it depend on the intracellular localization.

In COS7 cell coexpressing TrkA-Ros-ECFP and EYFP-SHP1-SH2, the fluorescence decay of ECFP could not be approximated in all regions of the cell with a monoexponential decay function and only a biexponential fit (with τ_s fixed to 2.0 ns) yielded satisfying χ^2 values (Fig. 5B). As discussed in more detail below, this finding indicates the existence of two populations of TrkA-Ros-ECFP. The mean lifetime in these cells was significantly ($P<0.05$) reduced compared with cells expressing TrkA-Ros-ECFP only ($\overline{\tau_m^c}$ = 1.69±0.03 ns, Fig. 5A,E) suggesting a certain level of constitutive association of both molecules, in agreement with the streak camera and spectroscopy measurements described above.

When cells coexpressing TrkA-Ros-ECFP and EYFP-SHP1-SH2 were subjected to stimulation with NGF, zones and clusters of short lifetimes could be detected in the cell periphery, indicating complex formation stimulated by NGF (Fig. 5B). Mean lifetimes of cells coexpressing TrkA-Ros-ECFP and EYFP-SHP1-SH2 were significantly ($P<0.05$) but only moderately decreased after NGF stimulation ($\overline{\tau_m^c}$ = 1.60±0.02 ns, Fig. 5E). Thus, owing to the already existing constitutive association, and despite local effects, NGF could not enhance the overall degree of association by much. These data were supported by measurements of living cells, which have the advantage that NGF induced changes are not averaged over the entire population, but can be followed up in individual cells. When cells were selected that exhibited intermediate or long mean lifetimes, which would be indicative of a low degree of constitutive association, a considerable decrease of τ_m^c could be observed (Fig. 6A,B). However, for all measurements made in living cells (n=7) the mean values ($\overline{\tau_m^c}$ = 1.71±0.09 ns before and $\overline{\tau_m^c}$ = 1.58±0.09 ns after application of NGF) were close to the respective values of fixed cells. ECFP lifetimes recovered to control values when the acceptor (EYFP) was photobleached (Fig. 6C), which indicates that the decrease in fluorescence lifetime observed after NGF stimulation was only due to FRET between TrkA-Ros-ECFP and EYFP-SHP1-SH2 and not to any other quenching process or photobleaching. In accordance with the lifetime imaging data, we also observed membrane accumulation of EYFP-SHP-1 derivatives with intact SH2 domain upon NGF-stimulation of living COS7 cells expressing TrkA-Ros-ECFP by laser scanning microscopy (Fig. 6D,E).

In Fig. 7 a more detailed analysis of the fluorescence decay is depicted, observed in each pixel after NGF-induced complex formation of TrkA-Ros-ECFP and EYFP-SHP1-SH2. As in the examples shown before, the fluorescence decay of some regions had to be approximated by a biexponential function to achieve a satisfying fit. Again, the fluorescence lifetime (τ_m) is predominantly decreased in the cell periphery (Fig. 7B, left)

and the distribution of τ_m over the entire cell exhibits two distinct peaks at 1.5 and 1.9 ns (Fig. 7C, left). As before, the slow lifetime component (τ_s) was set to the lifetime of unquenched ECFP. It can be attributed to the fraction of non-interacting TrkA-Ros-ECFP molecules, which are not subject to FRET. Associated TrkA-Ros-ECFP molecules, which were efficiently quenched by FRET, gave rise to the fast lifetime component (τ_f), which can be regarded as a characteristic property of associated molecules. Thus, the relative amplitudes of the fast (A_f) and slow (A_s) lifetime component provide a rough estimate for the fraction of interacting versus non-interacting molecules.
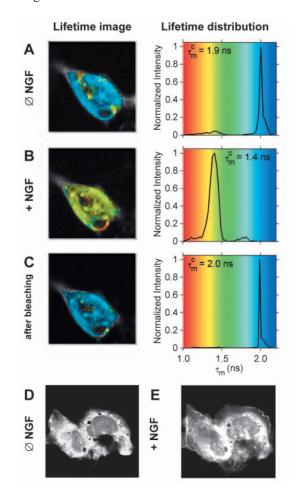

Fig. 6. Ligand-stimulated complex formation between SHP-1 and TrkA-Ros in living COS7 cells. (A) Left panel: fluorescence lifetime image of a COS7 cell coexpressing TrkA-Ros-ECFP and EYFP-SHP1-SH2. Amplitude weighted mean fluorescence lifetimes are encoded by color as specified in the right panels. Right panel: distribution of mean fluorescence lifetimes over the entire cell. (B) Lifetime image of the cell shown in A 40 minutes after stimulation with 100 ng/ml NGF. (C) Subsequent recording of the same cell after photobleaching of the acceptor (EYFP) with the Ar 514 nm line. ECFP fluorescence lifetimes recovered to control values. (D,E) COS7 cells expressing TrkA-Ros-ECFP and EYFP-SHP1-C455S before (D) and after (E) treatment with 100 ng/ml NGF for 20 minutes. Images were recorded by confocal LSM in the EYFP channel. Note that a fraction of the SHP1 derivative is enriched at the plasma membrane. Similar translocations were seen in 8 of 10 analyzed cells, but not upon mock-treatment or in cells expressing SHP1 variants with inactivated N-terminal SH2 domain.
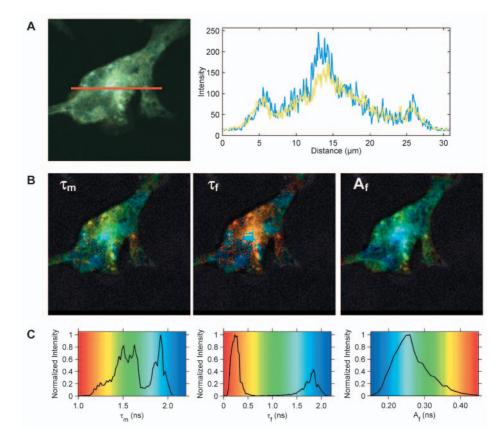
Fig. 7. Detailed analysis of lifetime components in NGF-stimulated cells. COS7 cells expressing TrkA-Ros-ECFP and EYFP-SHP1-SH2 were stimulated with 100 ng/ml NGF for 20 minutes. Cells were fixed and confocal and fluorescence lifetime images were recorded. (A) Left panel: LSM image with superimposed ECFP and EYFP channel. Right panel: the quantitative distribution of ECFP (blue curve) and EYFP (yellow curve) along the line depicted in the left panel is shown. (B) Color-coded images of the amplitude weighted mean lifetime (τ_m), the fast lifetime component (τ_f) and its amplitude (A_f). The color scale used is shown in the respective panels of C. (C) Distribution of the parameters visualized in B over the entire cell.

This interpretation is confirmed by visualization of the parameters recovered in the fit (Fig. 7B). In the pixels where τ_m is low, the amplitude (A_f) of the fast lifetime component (τ_f) is high, indicating that a high fraction of TrkA-Ros-ECFP molecules is subjected to FRET (and thus associated with EYFP-SHP1-SH2). By contrast, A_f is low in pixels where τ_m is close to the lifetime of unbound TrkA-Ros-ECFP, indicating that only a small fraction of TrkA-Ros-ECFP molecules is associated (Fig. 7B, right). In some pixels the values of τ_f were close to τ_s (Fig. 7B, middle, blue) and the biexponential fit converged to a quasi monoexponential decay. Accordingly, the distribution of τ_f exhibits two well separated peaks (Fig. 7C, middle). The first peak can be attributed to pixels in which complexes of TrkA-Ros-ECFP and EYFP-SHP1-SH2 are present and the second peak can be assigned to regions where the fraction of quenched (and associated) TrkA-Ros-ECFP molecules is minimal. Comparison of the lifetime images (Fig. 7B) with the confocal image and the intensity profile along a representative cross-section (Fig. 7A) shows that τ_m is not always decreased and that A_f is not always increased in pixels with high ECFP and EYFP fluorescence intensities. Thus, FRET between TrkA-Ros-ECFP and EYFP-SHP1-SH2 cannot merely be induced by high concentrations of both proteins. Only specific interaction of EYFP-SHP1-SH2 with TrkA-Ros-ECFP brings both fluorescence tags into close vicinity so that FRET occurs.

Role of Ros phosphotyrosines pY2267 and pY2327

In COS7 cells coexpressing the mutant TrkA-Ros-ECFP-Y2267F and EYFP-SHP1-SH2, the extent of constitutive complex formation is not significantly different from cells containing wild-type TrkA-Ros-ECFP and EYFP-SHP1-SH2 ($\overline{\tau_m^c}$ = 1.67±0.05 ns vs. 1.69±0.03 ns, Fig. 5E). Upon stimulation with NGF no significant change of the mean lifetime could be observed ($\overline{\tau_m^c}$ = 1.73±0.04 ns, Fig. 5D,E). Thus, loss of Y2267 abrogated the NGF-stimulated complex formation typically detectable with wild-type TrkA-Ros-ECFP. Similar data were observed in living cells ($\overline{\tau_m^c}$ = 1.68±0.10 ns before NGF-stimulation vs. 1.59±0.05 ns after NGF stimulation). By contrast, mutating Y2327 clearly reduced the level of constitutive complex formation ($\overline{\tau_m^c}$ = 1.87±0.07 ns, Fig. 5D,E). NGF-stimulation led to a significant ($P<0.05$) decrease of the mean lifetime to levels similar to wild-type TrkA-Ros-ECFP ($\overline{\tau_m^c}$ = 1.53±0.07 ns). Again these data could be confirmed by measurements in living cells ($\overline{\tau_m^c}$ = 1.85±0.05 ns before NGF-stimulation vs. 1.55±0.08 ns after NGF stimulation). Biochemical experiments supported a role of both pY2267 and pY2327 for interaction of SHP-1 with TrkA-Ros. Coimmunoprecipitation revealed a considerable degree of constitutive association of SHP-1 with TrkA-Ros in intact cells (Fig. 8A). NGF-stimulation enhanced the association to some extent, an effect which was lost in the Y2267F mutant. Mutation of Y2327 strongly reduced association, but NGF stimulation was still detectable. We have previously shown that the association of SHP-1 via pY2267 is important for the efficacy of TrkA-Ros dephosphorylation (Keilhack et al., 2001). Interestingly, as shown in Fig. 8B, Y2327F mutation also reduced the efficacy of TrkA-Ros dephosphorylation significantly. In summary, in intact cells both pY2267 and pY2327 contribute to TrkA-Ros-ECFP/SHP1-SH2 association

and SHP-1 mediated dephosphorylation. pY2327 seems to mediate mainly a constitutive association. When pY2327 is lost, pY2267 suffices to mediate ligand-dependent association. Both sites appear to play a complementary or cooperative role for TrkA-Ros interaction.
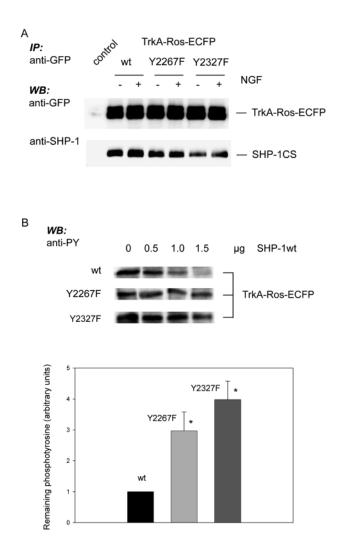

Fig. 8. Effect of binding site mutations on TrkA-Ros association with SHP-1 and dephosphorylation as revealed by biochemical methods. (A) TrkA-Ros-ECFP-wt or the respective mutants were coexpressed with catalytically inactive SHP-1CS in HEK293 cells. TrkA-Ros-ECFP was immunoprecipitated from cell lysates with anti-GFP antibodies, and associated SHP-1CS was detected with anti-SHP-1 antibodies. Control: IgG isotype precipitation. Consistent results were obtained in corresponding experiments using untagged TrkA-Ros. (B) Dephosphorylation of TrkA-Ros-ECFP or the respective mutants by coexpressed SHP-1-wt. TrkA-Ros-ECFP-wt or the YF mutants, as indicated, were expressed in HEK293 cells with or without different amounts of SHP-1 wild-type. Lysate aliquots were analyzed with anti-phosphotyrosine antibodies (4G10) for TrkA-Ros-ECFP phosphorylation. Expression levels of receptor and SHP-1 were comparable (not shown). The resulting bands for three independent experiments with a ratio of TrkA-Ros-ECFP:SHP-1 of approximately 1:2 were quantified, normalized to TrkA-Ros-ECFP expression levels, and relative ratios of tyrosine phosphorylation in presence or absence of SHP-1 were calculated (lower panel: means±s.e.m.; *significantly different from wild-type, $P<0.05$).

Discussion

Novel high-affinity binding sites for the SHP-1 SH2 domain

Characterization of the SHP-1 binding sites pY2267 and pY2327 on the Ros RTK revealed that both are of high affinity. pY2267 was sufficient to confer SHP-1 binding to the heterologous EGFR RTK. The sequences LNpY(2267)MVL and LNpY(2327)ACL correspond to the previously proposed consensus sequence for the SHP-1 N-terminal SH2 domain, hXpYhXh (h, hydrophobic) (Burshtyn et al., 1997; Pei et al., 1996). Using a phosphopeptide library approach, Beebe et al. have recently described two classes of phosphopeptide ligands for this domain: LXpY(M/F)X(F/M/L) (class I) and LXpYAXL (class II) (Beebe et al., 2000). The pY2267 and pY2327 sites match the consensus of class I and II, respectively. Beebe et al. also proposed two classes of binding sites for the SHP-1 C-terminal SH2 domain (Beebe et al., 2000) and pY2327 matches also the corresponding class I consensus (V/I/L)XpYAX(L/V). Therefore, it seems possible that SHP-1 binds to both sites simultaneously, via the tandem SH2 domains. The previous mutational analysis of SHP-1 binding to Ros in vitro revealed only participation of the N-terminal SH2 domain and of Ros pY2267 (Keilhack et al., 2001). By contrast, FRET measurements and biochemical experiments in intact cells described here support the view that also pY2327 is involved in complex formation between TrkA-Ros and SHP-1, mediating a constitutive interaction and contributing to efficient dephosphorylation. Since we found that a peptide containing the Y2327 site is only a poor substrate for Ros kinase it seems likely that Y2327 is phosphorylated by another tyrosine kinase in intact cells. Interestingly, the extent of constitutive association increased with prolonged starvation of the cells (data not shown) suggesting that this kinase may be more active under conditions of serum depletion. Phosphorylation of both Y2267 and Y2327 may potentially allow binding of SHP-1 to Ros via both SH2 domains. Our data are, however, more compatible with an alternative association of SHP-1 with either the pY2327 or the pY2267 site. Mutation of Y2327 abrogated constitutive association. Nevertheless, ligand-dependent association occurred and, based on the FRET measurements, reached levels similar to those of wild-type TrkA-Ros-ECFP. Thus, pY2267 appears sufficient to mediate efficient ligand-dependent association. It is tempting to speculate that, depending on the conditions of cell stimulation, phosphorylation of Y2327 may either enhance the efficiency of SHP-1 interaction, and thus cooperate with Y2267 in mediating downregulation of the signal. In addition, Y2327 may complement the function of Y2267 and play a role in downregulating spontaneous TrkA-Ros activity in the absence of ligand.

Database searches revealed that the pY2267 and pY2327 binding sites are conserved across human, mouse and chicken sequences and are unique for the Ros RTK (not shown). Equally high affinity binding sites for SHP-1 have not yet been described to occur in any other RTK. To our knowledge, a higher affinity binding than the ones described here, has only been observed for the SHP-1 N-terminal SH2 domain to PIRLα, a transmembrane adaptor protein in leukocytes (Mousseau et al., 2000). A direct interaction of SHP-1 has also been shown to occur with other RTKs, including the EGFR

(Keilhack et al., 1998), and c-Kit (Kozlowski et al., 1998). However, binding sequences in these receptors are, by comparison, of only low or moderate affinity. Binding of SHP-1 via adaptor molecules, in addition to direct binding, might be important in SHP-1-mediated regulation of these RTKs (Östman and Böhmer, 2001). Thus, interaction of Ros with SHP-1 stands out as an example of direct interaction, concomitant with negative regulation of signaling. Still, regulation of Ros signaling by SHP-1 might additionally occur through indirect mechanisms. Also, other PTPs might participate in Ros dephosphorylation. Interestingly, the Ros catalytic domain has a high homology to the insulin receptor kinase domain (Riethmacher et al., 1994; Sonnenberg-Riethmacher et al., 1996), including a conserved DYY motif in the activation loop. In its phosphorylated form, the latter sequence has been described as an efficient PTP1B substrate and it is possible that Ros is also a target for this ubiquitously expressed PTP (Salmeen et al., 2000). An interaction of one RTK with multiple PTPs has been recurrently discussed (Haj et al., 2003; Östman and Böhmer, 2001) and it may explain why single PTP knockouts have often no obvious RTK signaling phenotypes.

Visualization of target interaction for SHP-1

The high affinity of SHP-1 Ros interaction enabled us to visualize the complex formation between both partners in intact cells. Our data, mainly obtained by ECFP lifetime measurements, show a constitutive association of SHP-1 with TrkA-Ros upon coexpression, provided that the SHP-1 variant has an intact N-terminal SH2 domain. In addition, we show that a fraction of SHP-1 translocates to the plasma membrane in response to TrkA-Ros activation by NGF. To our knowledge, these results represent the first demonstration of a SHP-1–target interaction in intact cells. Complex formation between an RTK and a PTP has recently also been demonstrated by FRET for the EGFR and platelet-derived growth factor receptor (PDGFR) and for PTP1B (Haj et al., 2002). In the study of these authors, FRET was measured between GFP-tagged RTKs and a Cy3-labeled anti-PTP1B mAb. Interaction required ligand-triggered internalization and occurred only with the catalytically inactive PTP1B D181A mutant but was undetectable with wild-type PTP1B (Haj et al., 2002) suggesting a dominant role of the PTP1B catalytic domain for complex formation. In the case described here, the SHP-1 SH2 domain interaction with the Ros target is

obviously critical for complex formation. From the translocation experiments and lifetime imaging data it can be suggested that SHP-1 binds to activated Ros RTK in the plasma membrane. In contrast to PTP1B, no stringent binding of SHP-1 to any cellular substructure has yet been described. It thus may not be restricted to a certain cellular location for target interaction. Our analysis of constitutive interaction between SHP-1 and Ros shows, however, that intracellular complex formation also occurs. While a part of this interaction may be triggered by inappropriate localization of Ros in the used overexpression setting, it is possible that SHP-1 indeed functions to suppress intracellular signaling of newly synthesized and maturing RTK. SHP-1 is partly localized in a
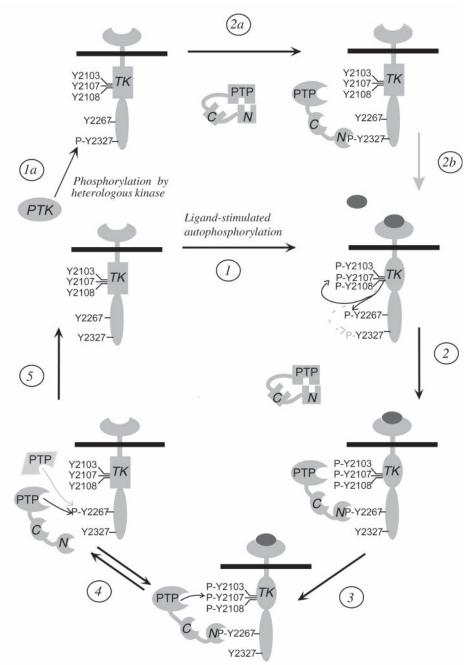

Fig. 9. Proposed model of Ros-SHP-1 interaction. For a discussion of the different steps, see text.

perinuclear compartment (Tenev et al., 2000) and thus in close proximity to newly synthesized RTKs.

Mechanism of RTK PTP complex decomposition and model of SHP-1/Ros interaction

Previous biochemical studies revealed that wild-type SHP-1-TrkA-Ros complexes are less stable than such of TrkA-Ros with catalytically inactive SHP-1 versions. The dephosphorylation studies described here suggest that this may not be due to SHP-1 mediated dephosphorylation of the SH2-domain binding site, but may rather be caused by dephosphorylation of activation loop phosphotyrosines and inactivation of the kinase. The pronounced SHP-1 activity against Ros activation loop phosphotyrosine(s) is an interesting observation that requires deeper investigation. For the insulin receptor, efficient dephoshorylation of the activation loop by PTP1B has been shown (Salmeen et al., 2000). Kinase inactivation, in contrast to dephosphorylation of SH2 domain binding sites, appears as an important general mechanism of PTP-mediated RTK regulation.

Taken together, our biochemical and FRET data support a model for SHP-1-Ros interaction as depicted in Fig. 9. (1) Ligand stimulation leads to Ros kinase activation and to phosphorylation of Y2267. (2) SHP-1 is recruited to phosphorylated Ros in the plasma membrane by high-affinity binding to the pY2267 sequence and is in turn activated. (3) SHP-1 dephosphorylates activation loop phosphotyrosines pY2103, pY2107 and pY2108 of Ros, which leads to kinase inactivation, provided the ligand is no longer present. (4) The binding sites are then eventually destroyed by dephosphorylation, mediated either (inefficiently) by SHP-1, or by other PTPs. (5) In turn, the SHP-1-Ros complex is decomposed. (1a) Even in the absence of a ligand, phosphorylation of Ros Y2327 by a heterologous protein tyrosine kinase can occur. (2a) This leads to constitutive complex formation, enabling SHP-1 to suppress spontaneous TrkA-Ros activation. (2b) The formed SHP-1/TrkA-Ros complexes may also undergo ligand activation, and pY2327-associated SHP-1 then contributes to TrkA-Ros dephosphorylation. In this setting, pY2627 and pY2327 may cooperate with respect to TrkA-Ros regulation by SHP-1.

Our data explain why Ros is an efficient target of SHP-1 in vivo. The differential and cooperative role of two high-affinity binding sites is an interesting aspect of this regulation mechanism and may apply also to other cases of SHP-1–target interaction.

References

Beebe, K. D., Wang, P., Arabaci, G. and Pei, D. (2000). Determination of the binding specificity of the SH2 domains of protein tyrosine phosphatase SHP-1 through the screening of a combinatorial phosphotyrosyl peptide library. *Biochemistry* **39**, 13251-13260.

Biskup, C., Kelbauskas, L., Zimmer, T., Benndorf, K., Bergmann, A., Becker, W., Ruppersberg, J. P., Stockklausner, C. and Klöcker, N. (2004a). Interaction of PSD-95 with potassium channels visualized by fluorescence-lifetime based resonance energy transfer imaging. *J. Biomed. Opt.* **9**, 753-759.

Biskup, C., Zimmer, T. and Benndorf, K. (2004b). Förster resonance energy transfer (FRET) between cardiac Na$^+$ channel subunits measured with a confocal microscope and a streak camera. *Nat. Biotechnol.* **22**, 220-224.

Bone, H., Dechert, U., Jirik, F., Schrader, J. W. and Welham, M. J. (1997). SHP1 and SHP2 protein-tyrosine phosphatases associate with betac after interleukin-3-induced receptor tyrosine phosphorylation. Identification of potential binding sites and substrates. *J. Biol. Chem.* **272**, 14470-14476.

Burshtyn, D. N., Yang, W., Yi, T. and Long, E. O. (1997). A novel phosphotyrosine motif with a critical amino acid at position –2 for the SH2 domain-mediated activation of the tyrosine phosphatase SHP-1. *J. Biol. Chem.* **272**, 13066-13072.

Chiarugi, P., Cirri, P., Taddei, M. L., Talini, D., Doria, L., Fiaschi, T., Buricchi, F., Giannoni, E., Camici, G., Raugei, G. et al. (2002). New perspectives in PDGF receptor downregulation: the main role of phosphotyrosine phosphatases. *J. Cell Sci.* **115**, 2219-2232.

Haglund, K., Sigismund, S., Polo, S., Szymkiewicz, I., di Fiore, P. P. and Dikic, I. (2003). Multiple monoubiquitination of RTKs is sufficient for their endocytosis and degradation. *Nat. Cell Biol.* **5**, 461-466.

Haj, F. G., Verveer, P. J., Squire, A., Neel, B. G. and Bastiaens, P. I. (2002). Imaging sites of receptor dephosphorylation by PTP1B on the surface of the endoplasmic reticulum. *Science* **295**, 1708-1711.

Haj, F. G., Markova, B., Klaman, L. D., Böhmer, F. D. and Neel, B. G. (2003). Regulation of receptor tyrosine kinase signaling by protein tyrosine phosphatase-1B. *J. Biol. Chem.* **278**, 739-744.

Hunter, T. (1998). The role of tyrosine phosphorylation in cell growth and disease. *Harvey Lect.* **94**, 81-119.

Keilhack, H., Tenev, T., Nyakatura, E., Godovac-Zimmermann, J., Nielsen, L., Seedorf, K. and Böhmer, F. D. (1998). Phosphotyrosine 1173 mediates binding of the protein-tyrosine phosphatase SHP-1 to the epidermal growth factor receptor and attenuation of receptor signaling. *J. Biol. Chem.* **273**, 24839-24846.

Keilhack, H., Müller, M., Böhmer, S. A., Frank, C., Weidner, K. M., Birchmeier, W., Ligensa, T., Berndt, A., Kosmehl, H., Günther, B. et al. (2001). Negative regulation of Ros receptor tyrosine kinase signaling. An epithelial function of the SH2 domain protein tyrosine phosphatase SHP-1. *J. Cell Biol.* **152**, 325-334.

Klingmüller, U., Lorenz, U., Cantley, L. C., Neel, B. G. and Lodish, H. F. (1995). Specific recruitment of SH-PTP1 to the erythropoietin receptor causes inactivation of JAK2 and termination of proliferative signals. *Cell* **80**, 729-738.

Kozlowski, M., Larose, L., Lee, F., Le, D. M., Rottapel, R. and Siminovitch, K. A. (1998). SHP-1 binds and negatively modulates the c-Kit receptor by interaction with tyrosine 569 in the c-Kit juxtamembrane domain. *Mol. Cell. Biol.* **18**, 2089-2099.

Majoul, I., Straub, M., Hell, S. W., Duden, R. and Soling, H. D. (2001). K_dEL-cargo regulates interactions between proteins involved in COPI vesicle traffic: measurements in living cells using FRET. *Dev. Cell* **1**, 139-153.

Mousseau, D. D., Banville, D., L'Abbe, D., Bouchard, P. and Shen, S. H. (2000). PILRalpha, a novel immunoreceptor tyrosine-based inhibitory motif-bearing protein, recruits SHP-1 upon tyrosine phosphorylation and is paired with the truncated counterpart PILRbeta. *J. Biol. Chem.* **275**, 4467-4474.

Östman, A. and Böhmer, F. D. (2001). Regulation of receptor tyrosine kinase signaling by protein tyrosine phosphatases. *Trends Cell Biol.* **11**, 258-266.

Pei, D., Lorenz, U., Klingmüller, U., Neel, B. G. and Walsh, C. T. (1994). Intramolecular regulation of protein tyrosine phosphatase SH-PTP1: a new function for Src homology 2 domains. *Biochemistry* **33**, 15483-15493.

Pei, D., Wang, J. and Walsh, C. T. (1996). Differential functions of the two Src homology 2 domains in protein tyrosine phosphatase SH-PTP1. *Proc. Natl. Acad. Sci. USA* **93**, 1141-1145.

Riethmacher, D., Langholz, O., Gödecke, S., Sachs, M. and Birchmeier, C. (1994). Biochemical and functional characterization of the murine ros protooncogene. *Oncogene* **9**, 3617-3626.

Salmeen, A., Andersen, J. N., Myers, M. P., Tonks, N. K. and Barford, D. (2000). Molecular basis for the dephosphorylation of the activation segment of the insulin receptor by protein tyrosine phosphatase 1B. *Mol. Cell* **6**, 1401-1412.

Schlessinger, J. (2000). Cell signaling by receptor tyrosine kinases. *Cell* **103**, 211-225.

Sonnenberg, E., Godecke, A., Walter, B., Bladt, F. and Birchmeier, C. (1991). Transient and locally restricted expression of the ros1 protooncogene during mouse development. *EMBO J.* **10**, 3693-3702.

Sonnenberg-Riethmacher, E., Walter, B., Riethmacher, D., Godecke, S. and Birchmeier, C. (1996). The c-ros tyrosine kinase receptor controls regionalization and differentiation of epithelial cells in the epididymis. *Genes Dev.* **10**, 1184-1193.

Tenev, T., Böhmer, S. A., Kaufmann, R., Frese, S., Bittorf, T., Beckers, T. and Böhmer, F. D. (2000). Perinuclear localization of the protein-tyrosine phosphatase SHP-1 and inhibition of epidermal growth factor-stimulated STAT1/3 activation in A431 cells. *Eur. J. Cell Biol.* **79**, 261-271.

Waltenberger, J., Uecker, A., Kroll, J., Frank, H., Mayr, U., Bjorge, J. D., Fujita, D., Gazit, A., Hombach, V., Levitzki, A. et al. (1999). A dual inhibitor of platelet-derived growth factor beta-receptor and Src kinase activity potently interferes with motogenic and mitogenic responses to PDGF in vascular smooth muscle cells. A novel candidate for prevention of vascular remodeling. *Circ. Res.* **85**, 12-22.

Yang, J., Liu, L., He, D., Song, X., Liang, X., Zhao, Z. J. and Zhou, G. W. (2002). Crystal structure of human protein tyrosine phosphatase SHP-1. *J. Biol. Chem.* **278**, 6516-6520.